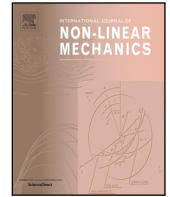




Contents lists available at ScienceDirect

International Journal of Non-Linear Mechanics

journal homepage: www.elsevier.com/locate/nlm

Edge effects in elastic bulging

Félix Benoist, Finn Box, Alain Goriely*

Mathematical Institute, University of Oxford, United Kingdom

A B S T R A C T

Elastic bulging occurs when an elastic material deforms through a small opening in a rigid boundary. This problem is complementary to the indentation problem where displacement is applied to a small part of an elastic material. Understanding bulging is crucial in a number of applications related to swelling such as the deformation of the brain following a decompressive craniectomy. In particular, it is known that large stresses develop close to the opening leading to potential material damage. To alleviate this problem, it is conceivable to modify the shape of the edge to reduce stress increases. Here, we study edge effects during planar bulging and show how an opening should be shaped to remove stress singularities.

1. Introduction

After a traumatic brain injury, intracranial pressure may increase [1] and create long lasting brain damage unless it is quickly reduced. If the intracranial pressure remains too large for an extended period of time, a routine, but highly invasive, treatment is *decompressive craniectomy* [2] where part of the skull is surgically removed [3] to allow the brain to swell uninhibitedly, thereby relieving pressure [4–7]. This operation is controversial because it creates potential axonal damage and local tissue damage near the skull opening [8,9].

A potential solution to reduce stress build-up at the opening is to insert a toric joint between the skull and the brain, which has the consequence of curving the edge and the elastic material [10]. We investigate the mechanical consequences of the implementation of a toric joint by examining bulging through an opening and the effect of the opening edges on the stress and strain inside a bulging elastic material.

Whereas indentation is the deformation of an elastic material due to the displacement of a small part of its boundary, bulging is the deformation of an elastic material through the opening of a rigid boundary. Unlike the case of indentation that has been studied extensively [11], bulging has received little attention in the literature and was only recently introduced as a generic problem motivated by medical concerns [12].

Here, we consider the bulging of a (linearly) elastic half-plane. For small deformations and in a planar geometry, the exact solution is derived from the theory of contact mechanics and we can explicitly study the deformations resulting from a sharp-edge and a curved-edge opening.

1.1. Preliminaries

We consider an elastic half plane $\Omega = \{x \in \mathbb{R}, z > 0\}$ subjected to a distributed load from a curved lip at the boundary. Inside the domain, the deformation is described by a displacement field $\mathbf{u} = (u_x, u_z) : \Omega \rightarrow \mathbb{R}^2$ such that a point originally at $\mathbf{x} \in \Omega$ displaces to a point at $(\mathbf{x} + \mathbf{u}) \in \mathbb{R}^2$. The (infinitesimal) strain tensor \mathbf{E} is

$$\mathbf{E} = \frac{1}{2} (\nabla \mathbf{u} + (\nabla \mathbf{u})^T). \quad (1.1)$$

As shown in Fig. 1, the boundary $\Gamma = \partial\Omega$ is split into two subsets where the elastic material is either in contact (Γ_c) or traction free ($\Gamma_f = \Gamma \setminus \Gamma_c$). On Γ_c the vertical displacement of the elastic material is constrained such that $u_z(x, z) = u_0(x)$, where u_0 is directly related to the profile of the plate. Note that apart from the curved edges, the plate is flat and rigid so that $u_0 = \delta$ is constant. At the boundary Γ_f , outside of Γ_c , the material is traction free.

The material is assumed to be a compressible, isotropic, initially unstressed, and linearly elastic solid with Young's modulus E and Poisson's ratio ν . Let \mathbf{T} be the Cauchy stress tensor, then the constitutive relationship between stresses and strains [13] is

$$\mathbf{T} = \frac{E}{1 + \nu} \left(\mathbf{E} + \frac{\nu}{1 - 2\nu} (\text{tr } \mathbf{E}) \mathbf{1} \right), \quad (1.2)$$

where $\mathbf{1}$ is the identity tensor.

For a given profile $u_0(x)$, the *bulging problem* consists in finding the displacement \mathbf{u} and the contact region Γ_c , such that

$$\text{div } \mathbf{T} = \mathbf{0}, \quad \mathbf{x} \in \Omega, \quad (1.3)$$

$$\mathbf{T} \mathbf{n} = \mathbf{0}, \quad (x, 0) \in \Gamma_f, \quad (1.4)$$

$$u_z(x) = u_0(x), \quad (x, 0) \in \Gamma_c, \quad (1.5)$$

* Corresponding author.

E-mail address: goriely@maths.ox.ac.uk (A. Goriely).<https://doi.org/10.1016/j.ijnonlinmec.2018.07.004>

Received 26 March 2018; Received in revised form 21 May 2018; Accepted 9 July 2018

Available online xxx

0020-7462/© 2018 The Authors. Published by Elsevier Ltd. This is an open access article under the CC BY license (<http://creativecommons.org/licenses/by/4.0/>).

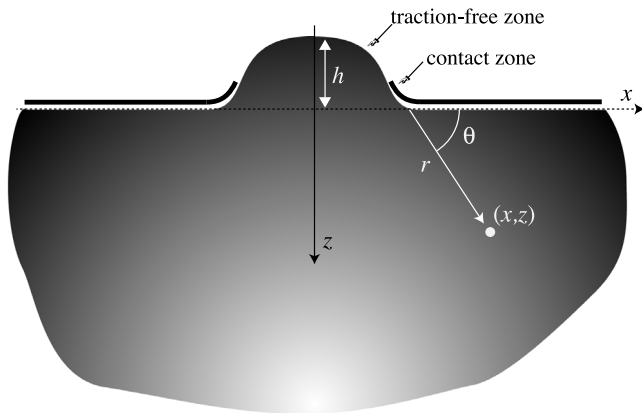


Fig. 1. An elastic material initially in a half-plane configuration is deformed by the vertical displacement of a rigid flat plate with curved edges. Doing so, it will develop a bulge. The contact zone and traction-free zone are indicated. Note that the point at which the material loses contact needs to be determined.

$$\mathbf{t} \cdot \mathbf{Tn} = 0, \quad (x, 0) \in \Gamma_c, \quad (1.6)$$

where \mathbf{n} (resp. \mathbf{t}) denotes the outward unit normal (resp. tangent) to Ω on Γ and the traction vector on Γ is given by \mathbf{Tn} . The last condition represents the frictionless constraint on the contact region.

1.2. The Cerruti–Flamant solution

Before we consider the case of a distributed load, we recall the classic Cerruti–Flamant solution for a half-space under a single normal point load P at the origin [14–16]. In this case, the radial stress is given

$$T_{rr} \equiv \mathbf{e}_r \cdot (\mathbf{T}\mathbf{e}_r) = -\frac{2P}{\pi} \frac{\sin \theta}{r}, \quad (1.7)$$

for a point located at $x = r \cos \theta, z = r \sin \theta$ (and $\mathbf{e}_r = (\cos \theta, \sin \theta)$) (see Fig. 1). This solution can be written in Cartesian coordinates as

$$T_{xx} = -\frac{2P}{\pi} \frac{x^2 z}{(x^2 + z^2)^2}, \quad (1.8)$$

$$T_{zz} = -\frac{2P}{\pi} \frac{z^3}{(x^2 + z^2)^2}, \quad (1.9)$$

$$T_{xz} = 0. \quad (1.10)$$

1.3. The Cerruti–Flamant solution as a Green’s function

Next, we assume that we have a distributed load. Since the contact is assumed to be frictionless, we have $p_x = 0$ which leads us to set $p(x) \equiv p_z(x)$, and we only consider symmetric loads i.e. $p(-x) = p(x) \forall x$. Then, the Cerruti–Flamant solution for the point load problem can be used as a Green’s function for a distributed normal force $p(x)dx$ on an element dx at each point on the surface.

$$T_{xx} = -\frac{2z}{\pi} \int_{-\infty}^{\infty} \frac{p(s)(x-s)^2}{((x-s)^2 + z^2)^2} ds, \quad (1.11)$$

$$T_{zz} = -\frac{2z^3}{\pi} \int_{-\infty}^{\infty} \frac{p(s)}{((x-s)^2 + z^2)^2} ds, \quad (1.12)$$

$$T_{xz} = -\frac{2z^2}{\pi} \int_{-\infty}^{\infty} \frac{p(s)(x-s)}{((x-s)^2 + z^2)^2} ds. \quad (1.13)$$

Using (1.1)–(1.2) at the surface $z = 0$, the displacement field $(u_x(x), u_z(x))$

$\equiv \mathbf{u}(x, 0)$ is related to the pressure field $p(x)$ as follows

$$\forall x \in \mathbb{R}, \quad \begin{cases} u_x(x) = \frac{B}{2} \int_S p(s) \operatorname{sgn}(x-s) ds \\ u_z(x) = -A \int_S p(s) \ln|x-s| ds, \end{cases} \quad (1.14)$$

where S is the subset of \mathbb{R} where contact is established ($S = \{x \in \mathbb{R} | (x, z) \in \Gamma_c\}$) and

$$A = \frac{2}{\pi} \frac{1-\nu^2}{E}, \quad B = \frac{(1+\nu)(1-2\nu)}{E}. \quad (1.15)$$

In the bulging problem, S is the union of two unbounded set $S = (-\infty, -a] \cup [a, \infty)$. Further since the derivative of the sign function can be expressed in the sense of distribution by Dirac’s delta: $d \operatorname{sgn}(x)/dx = 2\delta(x)$, differentiating (1.14) with respect to x leads to the following system of equations

$$\forall x \in \mathbb{R}, \quad \begin{cases} \frac{du_x}{dx} = Bp(x) \\ \frac{du_z}{dx} = -A \left(\int_{-\infty}^{-a} + \int_a^{\infty} \right) \frac{p(s)}{x-s} ds. \end{cases} \quad (1.16)$$

These relations directly connect the applied load to the surface displacement gradient. If the displacements are specified at the surface, the pressure needed to maintain this displacement is obtained by solving this system of equations. Once the pressure is known, the system (1.11)–(1.13) gives the stress at all points, from which the strains and displacements can be obtained. Notice that if the material is incompressible (i.e. $\nu = 1/2$), then $B = 0$.

1.4. Calculations of the pressure and the displacement

Since $u_z = u_0(x)$ is known in the contact zone, we have

$$\left(\int_{-\infty}^{-a} + \int_a^{\infty} \right) \frac{p(s)}{x-s} ds = -\frac{1}{A} \frac{du_0}{dx}(x) \equiv f(x), \quad |x| \geq a. \quad (1.17)$$

Mathematically, the problem is then to solve

$$\left(\int_{-\infty}^{-a} + \int_a^{\infty} \right) \frac{p(s)}{x-s} ds = f(x), \quad |x| \geq a, \quad (1.18)$$

for p . This is a singular integral equation of the first kind with a gap. This is not a standard problem for which solutions are readily available. In Appendix A, we use ideas from [17] to obtain the general homogeneous solutions (in the case where $f(x) = 0$) and, in Appendix B, we show how to obtain the solution for a particular $f(x)$ corresponding to a curved edge.

1.4.1. Sharp edges

We consider a uniform displacement δ in Γ_c . Therefore f vanishes identically and the pressure is given by the even homogeneous solution p_{even} of (1.18) as given in Appendix A.1:

$$p(s) = \frac{cE}{2} \frac{|s|}{\sqrt{s^2 - a^2}}, \quad |s| \geq a, \quad (1.19)$$

where $c > 0$ is an arbitrary dimensionless constant (note that the solution given in [12] contains typos that have been corrected here). From p , we find the derivative of the displacement in the bulging area i.e. outside of Γ_c :

$$\frac{du_z}{dx} = -2Ax \int_a^{\infty} \frac{p(s)}{x^2 - s^2} ds = Ax \frac{cE}{2} \frac{\pi}{\sqrt{a^2 - x^2}}, \quad |x| \leq a \quad (1.20)$$

and the vertical displacement is therefore

$$u_z(x) = \delta - c(1-\nu^2)\sqrt{a^2 - x^2}, \quad |x| \leq a, \quad (1.21)$$

in which the constant c is related to both the height $h = c(1-\nu^2)a$ and the area of the bulge $A_b = \pi ah/2$. We note that, remarkably, we recover the same expression as for the axisymmetric case for the bulging of a half-space [12] and that the shape of the bulge is an *ellipsoid of revolution* in three dimensions. The vertical displacement and the normal pressure at the surface are shown in Fig. 2 for $\delta = 0$. Note that the pressure is infinite at the edges.

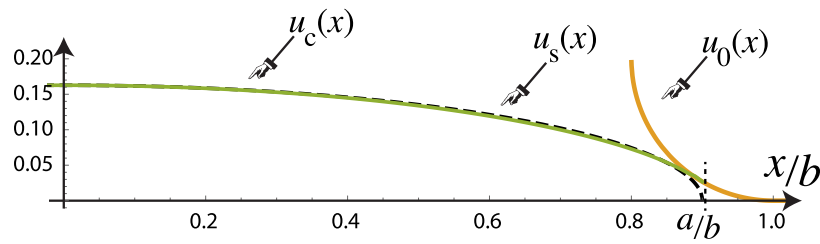


Fig. 6. Comparison of the displacement generated by a sharp edge, u_s (dashed) with the displacement u_c (solid green online) generated by a curved edge $u_0(x)$ (orange online). Here $a/b = 0.9$ and $R/b = 0.2$. The values are chosen so that $u_s(0) = u_c(0)$. We conclude that the displacements for a curved edge are very close to those generated by a sharp edge of a slightly smaller radius. (For interpretation of the references to color in this figure legend, the reader is referred to the web version of this article.)

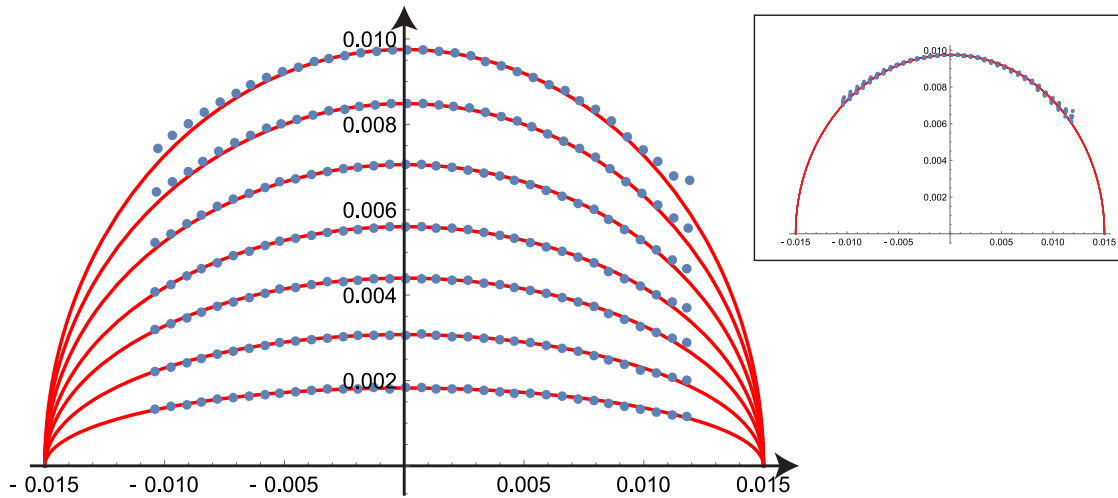


Fig. 7. Bulge solution with curved edges. Comparison between the analytical solution and experimental bulging (parameters given in Appendix, all values on the axes are in meters). Note that since the profile with straight and curved edges are almost identical, the analytical solution shown here is the simpler straight edge case.

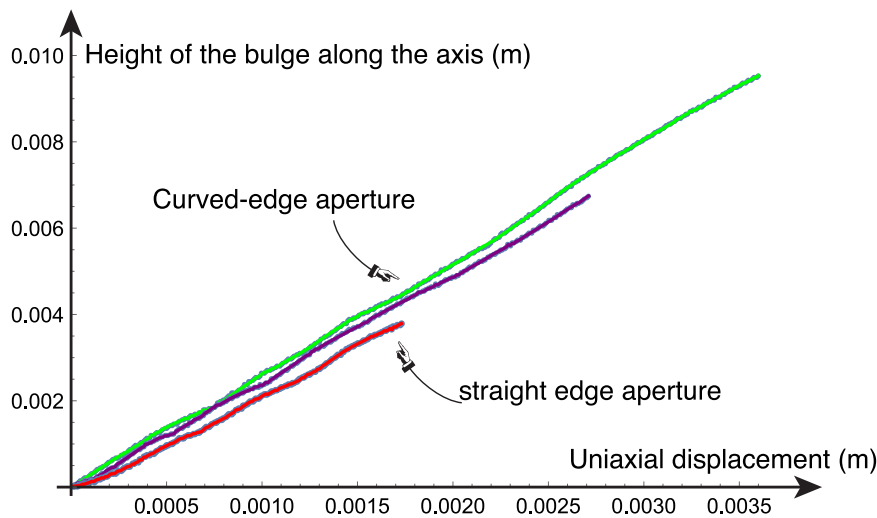


Fig. 8. Profile height as a function of the uniaxial compression (corresponding to an increasing swelling volume) for curved-edge and straight-edge apertures. The experimental data can be found in the supplemental material file (ExpData_Fig8.csv).

For $r \ll a$, shear stress is approximated at the lowest order in \bar{r} by

$$\sigma_{xz}^{app} = \frac{cE \sin \theta}{8 \sqrt{\bar{r}}} (\cos \theta \sqrt{1 + \cos \theta} - \sin \theta \sqrt{1 - \cos \theta}). \quad (1.28)$$

We recover the well-known scaling law $r^{-1/2}$ of stress around the singularity [18].

Let τ_{crit} be the critical value of shear stress past which damage occurs. We introduce the dimensionless parameter $K = cE/8\tau_{crit}$ to measure the extent of the damage zone. The shape of a damage drop is then defined by the polar curve

$$\bar{r}(\theta) = K^2 \sin^2 \theta (1 + \cos 3\theta), \quad 0 \leq \theta \leq \pi, \quad (1.29)$$

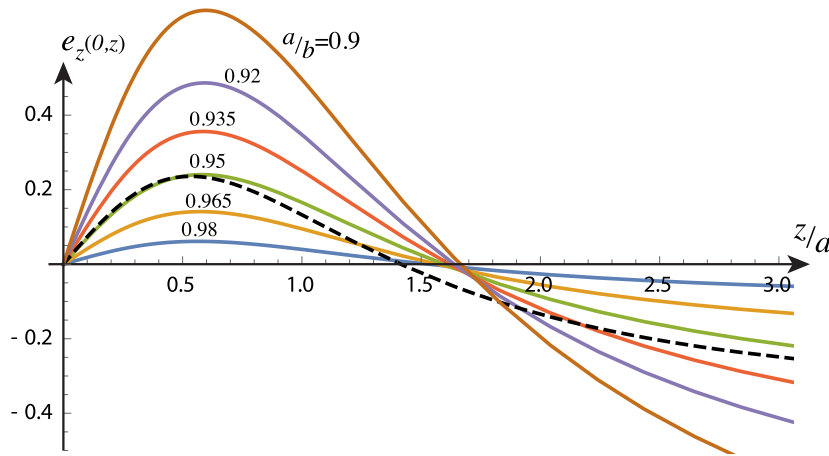


Fig. 15. Vertical strain for $\nu = 0.5$ and $c = 1.5$ in the sharp-edge case (black dashed) and in the curved-edge case for $a/b \in \{0.9, 0.92, 0.935, 0.95, 0.965, 0.98\}$ (smaller values lead to larger strains).

of the interface oscillating away from the contact). Yet, these effects seem to be concentrated close to the contact boundary whereas the profile away from it is mostly well described by the linear theory. The unreasonable effectiveness of the linear theory in Hertz-like problem is well known [24,25] but not yet understood. For our problem, in previous papers we have shown that the linear theory for bulging provides excellent agreement with finite-element simulations of non-linear materials in planar, cylindrical, and spherical geometries [5–7]. Here, we also provide experimental validations showing that the linear solution provides excellent predictions for displacement of the same order as the radius of the opening (See Fig. 7).

Going back to the original motivation, it should be clear that decompressive craniectomy is an extremely complex physiological process. Yet, basic physical ideas emerge from our highly idealized system and we expect our results concerning the shape of the bulge, the singularities of the stresses and the orientation of the damage drops to be generic for any type of bulging problem. Importantly, large stresses are generated at the opening, but, as shown here, these stresses can be partially mitigated by curved edges. However, Fletcher et al. [10] showed that in practice, the chaffer profile may not have much of an influence. A possible physical process to further mitigate these high stresses would be to employ a flexible toric joint that would extend the contact zone while providing some elasticity.

Acknowledgment

The support for Alain Goriely by the Engineering and Physical Sciences Research Council of Great Britain under research grant EP/R020205/1 is gratefully acknowledged.

Appendix A. The homogeneous solution to the singular integral equation

Consider the domain $S = (-\infty, -a] \cup [a, \infty)$ and an integrable function $f(x) : x \in S \rightarrow \mathbb{R}$. We are interested in finding the general solution to following singular integral equation with gap:

$$\left(\int_{-\infty}^{-a} + \int_a^{\infty} \right) \frac{p(s)}{x-s} ds = f(x), \quad |x| \geq a, \tag{A.1}$$

We first look for homogeneous solutions when pressure p is either an even or odd function of x .

A.1. p even

If p is even, we can rewrite the integral in (A.1) as

$$\left(\int_{-\infty}^{-a} + \int_a^{\infty} \right) \frac{p(s)}{x-s} ds = \int_a^{\infty} p(s) \left(\frac{1}{x-s} + \frac{1}{x+s} \right) ds$$

$$= 2x \int_a^{\infty} \frac{p(s)}{x^2 - s^2} ds. \tag{A.2}$$

Then the integral equation (A.1) is

$$\int_a^{\infty} \frac{p(s)}{x^2 - s^2} ds = \frac{f(x)}{2x}, \quad |x| \geq a. \tag{A.3}$$

Following [26], we introduce new $x^2 = u$ and $s^2 = v$, so that (A.3) reads now

$$\int_{a^2}^{\infty} \frac{P(v)}{u-v} dv = F(u), \quad |u| \geq a^2, \tag{A.4}$$

where

$$P(v) = \frac{p(\sqrt{v})}{\sqrt{v}} \quad \text{and} \quad F(u) = \frac{f(\sqrt{u})}{\sqrt{u}}. \tag{A.5}$$

From [17], we find that the solution of (A.4) is given by

$$P(v) = \frac{c_0}{\sqrt{v-a^2}} + \frac{1}{\pi^2} \int_{a^2}^{\infty} \sqrt{\frac{u-a^2}{v-a^2}} \frac{F(u)}{u-v} du, \tag{A.6}$$

where c_0 is a real constant. Hence the pressure is

$$p(s) = \frac{c_0 s}{\sqrt{s^2 - a^2}} + \frac{2s}{\pi^2} \int_a^{\infty} \sqrt{\frac{x^2 - a^2}{s^2 - a^2}} \frac{f(x)}{x^2 - s^2} dx, \quad s \geq a. \tag{A.7}$$

In the case $f(x) = 0$, we extract from this last expression the even kernel

$$p_{\text{even}}(s) = \frac{c_0 |s|}{\sqrt{s^2 - a^2}}, \quad |s| \geq a. \tag{A.8}$$

A.2. p odd

We enforce the condition that p is odd:

$$\left(\int_{-\infty}^{-a} + \int_a^{\infty} \right) \frac{p(s)}{x-s} ds = \int_a^{\infty} p(s) \left(\frac{1}{x-s} - \frac{1}{x+s} \right) ds = - \int_a^{\infty} \frac{p(s)}{x^2 - s^2} 2s ds. \tag{A.9}$$

Then (A.1) is rewritten

$$\int_a^{\infty} \frac{p(s)}{x^2 - s^2} 2s ds = f(x), \quad |x| \geq a. \tag{A.10}$$

Using the same transformation $x^2 = u$ and $s^2 = v$, (A.10) becomes

$$\int_{a^2}^{\infty} \frac{p(\sqrt{v})}{u-v} dv = f(\sqrt{u}), \quad |u| \geq a^2. \tag{A.11}$$

Its solution is [17]:

$$p(\sqrt{v}) = \frac{c_1}{\sqrt{v-a^2}} + \frac{1}{\pi^2} \int_{a^2}^{\infty} \sqrt{\frac{u-a^2}{v-a^2}} \frac{f(\sqrt{u})}{u-v} du, \tag{A.12}$$

where c_1 is a real constant. Hence the pressure is given by

$$p(s) = \frac{c_1}{\sqrt{s^2 - a^2}} + \frac{2}{\pi^2} \int_a^\infty \sqrt{\frac{x^2 - a^2}{s^2 - a^2}} \frac{xf(x)}{x^2 - s^2} dx, \quad s \geq a, \quad (\text{A.13})$$

from which we extract the odd homogeneous solution:

$$p_{\text{odd}}(s) = \frac{c_1 \operatorname{sgn}(s)}{\sqrt{s^2 - a^2}}, \quad |s| \geq a. \quad (\text{A.14})$$

Appendix B. Non-homogeneous solutions to the singular integral equations

The previous analysis provides a way to identify homogeneous solutions to the singular integral equations. Expressions (A.7) and (A.13) can also be used to find some non-homogeneous solutions. However, these expressions do not capture all solutions. In particular in the case of a curved edge, we notice that the non-homogeneous parts appearing in both expressions vanish identically. Thus we must solve equation (A.1) in a different way. Here, we use the following result from [17], valid for an inhomogeneous term defined on a finite domain of the form:

$$f(x) = \begin{cases} 0, & |x| \geq b \\ \frac{x-b}{AR}, & a \leq x \leq b \\ \frac{x+b}{AR}, & -b \leq x \leq -a, \end{cases} \quad (\text{B.1})$$

Then the pressure is

$$p(s) = \frac{\operatorname{sgn}(s)}{\pi^2 \sqrt{s^2 - a^2}} \left[c_1 + \left(\int_{-\infty}^{-a} + \int_a^\infty \right) \frac{f(t) \sqrt{t^2 - a^2} \operatorname{sgn}(t)}{t - s} dt \right] \\ = \frac{\operatorname{sgn}(s)}{\pi^2 AR \sqrt{s^2 - a^2}} \\ \times \left[c_1 + \underbrace{\int_{-b}^{-a} \frac{(-t-b) \sqrt{t^2 - a^2}}{t - s} dt + \int_a^b \frac{(t-b) \sqrt{t^2 - a^2}}{t - s} dt}_{=I(s)} \right], \quad (\text{B.2})$$

where we recognize the odd homogeneous solution. The explicit evaluation of this integral gives

$$I(s) = -\sqrt{s^2 - a^2} \left(s \ln \left| \frac{b^2 - 2a^2 + s^2 + 2\sqrt{(b^2 - a^2)(s^2 - a^2)}}{b^2 - s^2} \right| \right. \\ \left. + b \ln \left| \frac{b-s}{b+s} \frac{a^2 + bs - \sqrt{(b^2 - a^2)(s^2 - a^2)}}{a^2 - bs - \sqrt{(b^2 - a^2)(s^2 - a^2)}} \right| \right) \\ + 2s \left(\sqrt{b^2 - a^2} + b \ln \frac{a}{b + \sqrt{b^2 - a^2}} \right). \quad (\text{B.3})$$

When adding the even kernel, we obtain the general solution

$$p(s) \pi^2 AR = \frac{c_1 \operatorname{sgn}(s)}{\sqrt{s^2 - a^2}} + 2 \frac{|s|}{\sqrt{s^2 - a^2}} \left(c_0 + \sqrt{b^2 - a^2} + b \ln \frac{a}{b + \sqrt{b^2 - a^2}} \right) \\ - |s| \ln \left| \frac{b^2 - 2a^2 + s^2 + 2\sqrt{(b^2 - a^2)(s^2 - a^2)}}{b^2 - s^2} \right| \\ - b \operatorname{sgn}(s) \ln \left| \frac{b-s}{b+s} \frac{a^2 + bs - \sqrt{(b^2 - a^2)(s^2 - a^2)}}{a^2 - bs - \sqrt{(b^2 - a^2)(s^2 - a^2)}} \right|. \quad (\text{B.4})$$

Physically, we are looking for a non-divergent even solution. Therefore, we choose $c_1 = 0$ and c_0 such that $p(a) = p(-a)$ does not diverge:

$$c_0 + \sqrt{b^2 - a^2} + b \ln \frac{a}{b + \sqrt{b^2 - a^2}} = 0. \quad (\text{B.5})$$

Taken together, the solution for the pressure is

$$p(s) = -\frac{1}{\pi^2 AR} \left(|s| \ln \left| \frac{b^2 - 2a^2 + s^2 + 2\sqrt{(b^2 - a^2)(s^2 - a^2)}}{b^2 - s^2} \right| \right. \\ \left. + b \operatorname{sgn}(s) \ln \left| \frac{b-s}{b+s} \frac{a^2 + bs - \sqrt{(b^2 - a^2)(s^2 - a^2)}}{a^2 - bs - \sqrt{(b^2 - a^2)(s^2 - a^2)}} \right| \right). \quad (\text{B.6})$$

Appendix C. Experimental details

Bulging experiments were performed by compressing confined elastic solids using a plate with a circular aperture. The solid is confined on all faces except for a circular opening in the top plate. As the plate is displaced (axial compression) the solid is free to expand through the circular opening. Under this compression, the soft solid bulged through the aperture permitting measurement of the axisymmetric deformation profile.

The experimental sample, of $R = 45$ mm and $H = 20.5$ mm, was fabricated from poly-vinyl siloxane (Elite Double 8, Zhermack). The PVS sample was produced by mixing together a base polymer and crosslinker in a ratio of 9:1, which resulted in soft solid with Young's modulus $E = 40$ kPa and Poisson's ratio $\nu = 0.5$. After thorough mixing, and while still liquid, the sample was degassed in a vacuum chamber before being left to cure at room temperature inside a cylindrical container, of radius 45 mm and height 30 mm, with no lid. Prior to compressive testing the Young's modulus of the sample was measured by performing flat punch indentation experiments using a custom-built structural testing machine. The sample was positioned on a precision micro-balance (Pioneer PA64C Analytic Balance, Ohaus) and indented by a cylindrical indenter, of diameter $2r_i = 1.25$ mm, connected to a linear actuator (M228.10S, Physik Instrumente) and driven by a computer-controlled stepper motor. Simultaneous readings of both the mass, m , and indentation, δ_i , provided a stress-strain curve from which the Young's modulus, E , could be calculated via $F = 2r_i E^* \delta_i$, where $F = mg$, $E = E^*(1 - \nu^2)$ and ν is the Poisson's ratio of the material.

Confined inside the container, the soft solid was subject to axial compression by a circular plate of radius 44 mm with a circular aperture of radius $b = 15$ mm located at its center. To investigate the effect of edges on bulging, tests were performed with plates that had apertures with straight edges and apertures with a radii of curvature $R = 2$ mm and $R = 3$ mm. The plates, and the container that held the sample, were fabricated from ABS plastic using a 3D printer (MakerBot) with a resolution of 0.2 mm. The plate was attached to a computer-controlled linear actuator (M229.26S, Physik Instrumente) with a precision of $\pm 0.1 \mu\text{m}$, that moved at $10 \mu\text{m/s}$, applying an axial compression to the sample. Under compression, the soft solid bulged through the central aperture and the axisymmetric deformation profile was measured by imaging a line along the center of the sample. The line was approximately 1 mm wide, made from the same material, and with the same E , as the bulk and colored using an oil-based dye to contrast the rest of the sample. The line was imaged using a DSLR camera (D7000, Nikon), with a spatial resolution of 0.02 mm/pixel, positioned at 45 degrees to the horizontal and orthogonal to the line, at a rate of 1 fps. The line was detected in images using image processing techniques in Matlab, and compared to an undeformed reference line obtained for zero compression, resulting in measurements of the deformation profile accurate to 0.1 mm. The profiles shown in this paper were obtained for fixed values of axial compression in the range of 0.5 mm to 3.5 mm in 0.5 mm increments; in Fig. 7 for a curved-edge aperture of $R = 3$ mm.

Appendix D. Supplementary data

Supplementary material related to this article can be found online at <https://doi.org/10.1016/j.ijnonlinmec.2018.07.004>.

References

- [1] A. Marmarou, R.L. Anderson, J.D. Ward, S.C. Choi, H.F. Young, H.M. Eisenberg, M.A. Foulkes, L.F. Marshall, J.A. Jane, Impact of ICP instability and hypotension on outcome in patients with severe head trauma instability and hypotension on outcome in patients with severe head trauma, *J. Neurosurg.* (1991).
- [2] R.G. Ellenbogen, S.I. Abdulrauf, L.N. Sekhar, *Principles of Neurological Surgery*, Elsevier, Saunders, 2012.
- [3] J.F. Soustiel, G.E. Sviri, E. Mahamid, V. Shik, S. Abeshaus, M. Zaaroor, Cerebral blood flow and metabolism following decompressive craniectomy for control of increased intracranial pressure, *Neurosurgery* 67 (1) (2010) 65–72.

- [4] A. Goriely, M.G.D. Geers, G.A. Holzapfel, J. Jayamohan, A. Jérusalem, S. Sivaloganathan, W. Squier, J.A.W. van Dommelen, S.L. Waters, E. Kuhl, Mechanics of the brain: perspectives, challenges, and opportunities, *Biomech. Model. Mechanobiol.* 14 (2015) 931.
- [5] J. Weickenmeier, C. Butler, P.G. Young, A. Goriely, E. Kuhl, The mechanics of decompressive craniectomy: Personalized simulations, *Comput. Methods Appl. Mech. Engrg.* (2016).
- [6] J. Weickenmeier, E. Kuhl, A. Goriely, The mechanics of decompressive craniectomy: Bulging in idealized geometries, *J. Mech. Phys. Solids* (2016).
- [7] J. Weickenmeier, P. Saez, C.A.M. Butler, P.G. Young, A. Goriely, Ellen Kuhl, Bulging brains, *J. Elasticity* 129 (1–2) (2017) 197–212.
- [8] D.J. Cooper, J.V. Rosenfeld, L. Murray, Y.M. Arabi, A.R. Davies, P. D'Urso, T. Kossman, J. Ponsford, I. Seppelt, P. Reilly, R. Wolfe, Decompressive craniectomy in diffuse traumatic brain injury, *New England J. Med.* 364 (16) (2011) 1493–1502.
- [9] A.G. Koliias, P.J. Kirkpatrick, P.J. Hutchinson, Decompressive craniectomy: past, present and future, *Nat. Rev. Neurol.* (2013).
- [10] Tim L. Fletcher, Barbara Wirthl, Angelos G. Koliias, Hadie Adams, Peter J.A. Hutchinson, Michael P.F. Sutcliffe, Modelling of brain deformation after decompressive craniectomy, *Ann. Biomed. Eng.* (2016) 1–15.
- [11] J.R. Barber, *Elasticity*, Springer, 1992.
- [12] A. Goriely, J. Weickenmeier, E. Kuhl, Stress singularities in swelling soft solids, *Phys. Rev. Lett.* 117 (13) (2016) 138001.
- [13] A. Goriely, *The Mathematics and Mechanics of Biological Growth*, Springer Verlag, New York, 2017.
- [14] V. Cerruti, Ricerche intorno all' equilibrio de'corpi elastici isotropi, *R. Accad. Lincei Mem. Cl. Sci. Fis. Mat. E Nat.* 3 (13) (1882) 81–122.
- [15] A. Flamant, Sur la répartition des pressions dans un solide rectangulaire chargé transversalement, *C. R. Acad. Sci. Paris* 114 (1892) 1465–1468.
- [16] D.J. Unger, Similarity solution of the flamant problem by means of a one-parameter group transformation, *J. Elasticity Phys. Sci. Solids* 66 (1) (2002) 93–97.
- [17] A. Chakrabarti, S.C. Martha, Methods of solution of singular integral equations, *Math. Sci.* 6 (1) (2012) 15.
- [18] K.L. Johnson, *Contact Mechanics*, Cambridge University Press, 1987.
- [19] Paul G. Warne, Debra A. Polignone, Solutions for an infinite compressible nonlinearly elastic body under a line load, *Quart. Appl. Math.* 54 (2) (1996) 317–326.
- [20] Adair Aguiar, Roger Fosdick, A singular problem in incompressible nonlinear elastostatics, *Math. Models Methods Appl. Sci.* 10 (08) (2000) 1181–1207.
- [21] Adair Aguiar, Roger Fosdick, Self-intersection in elasticity, *Int. J. Solids Struct.* 38 (28–29) (2001) 4797–4823.
- [22] Ethan T. Coon, Debra Polignone Warne, Paul G. Warne, Asymptotic analysis of finite deformation in a nonlinear transversely isotropic incompressible hyperelastic half-space subjected to a tensile point load, *J. Elasticity* 75 (3) (2004) 197–228.
- [23] V.M. Mal'kov, Yu.V. Mal'kova, Analysis of a stress singularity in a non-linear flamant problem for certain models of a material, *J. Appl. Math. Mech.* 72 (4) (2008) 468–474.
- [24] G.M. Pharr, W.C. Oliver, F.R. Brotzen, On the generality of the relationship among contact stiffness, contact area, and elastic modulus during indentation, *J. Mater. Res.* 7 (3) (1992) 613–617.
- [25] Andong He, John S. Wettlaufer, Hertz beyond belief, *Soft Matter* 10 (13) (2014) 2264–2269.
- [26] S. Banerjee, B.N. Mandal, Solution of a singular integral equation in a double interval arising in the theory of water waves, *Appl. Math. Lett.* (1993).